

Journal of Aerosol Science
Heterogeneity in lobar and near-acini deposition of inhaled aerosol in the mouse lung
--Manuscript Draft--

Manuscript Number:	
Article Type:	VSI: Inhaled Aerosol Dosimetry
Section/Category:	Drug Delivery & Medical Applications of Aerosols
Keywords:	hot spots; spatial heterogeneity; particle deposition
Corresponding Author:	Chantal Darquenne University of California, San Diego La Jolla, California United States
First Author:	Wanjun Gu
Order of Authors:	Wanjun Gu Chantal Darquenne
Abstract:	Laboratory animals are often used to derive health risk from environmental exposure or to assess the therapeutic effect of a drug delivered by inhaled therapy . Knowledge of the in-situ distribution of deposited particles on airway and alveolar surfaces is essential in any assessment of these effects. A unique database including both high-resolution lung anatomy and deposition data in four strains of laboratory mice have been recently made publicly available to the research community (https://doi.org/10.25820/9arg-9w56). Using these data, we investigated the effect of particle size on the distribution of deposited particles at the lobar and near-acini level. Analysis was performed on a total of 33 mice where 3, 16 and 14 animals were exposed to 0.5µm, 1µm and 2µm particles, respectively. Ratio of normalized deposition to normalized volume was calculated for each lobe (DV lobe). At the near-acini level, the skew and standard deviation of the frequency distribution of particle deposition were calculated. Significant deviation above 1 was found for DV ratio in the cranial lobe (DV cranial). DV Middle , DV caudal and DV accessory were all significantly <1 and lower than ($p<0.01$). At the near-acini level, skew and standard deviation were positively correlated with particle size and the presence of hot spots (high deposition) were mainly found in the apical region of the lung. These results highlight the uneven distribution of deposited particles in the mouse lung. Thus, depending on the lung sample, individual analysis to determine overall deposition may either underestimate or overestimate total lung burden, at least for micron-sized particles.
Suggested Reviewers:	Robb Glenny glenny@uw.edu Otmar Schmid otmar.schmid@helmholtz-muenchen.de
Opposed Reviewers:	



Chantal Darquenne, PhD

Professor of Medicine

Section of Physiology

Division of Pulmonary, Critical Care & Sleep Medicine

cdarquenne@health.ucsd.edu

May 19, 2020

To the Editor of the *Journal of Aerosol Science*:

Please find enclosed a manuscript to be considered for publication in the special issue of the *Journal of Aerosol Science* dedicated to “Inhaled Aerosol Dosimetry”. The manuscript describes results that were presented at the third Inhaled Aerosol Dosimetry Conference held in October 2019 at the Arnold and Mabel Beckman Center of the National Academies of Sciences and Engineering in Irvine, California.

Sincerely Yours,

A handwritten signature in blue ink that reads "Darquenne". The signature is fluid and cursive, with the first name "Chantal" and the last name "Darquenne" connected.

Chantal Darquenne, PhD
Professor of Medicine

Highlights

- Volume-normalized deposition is highest in the cranial lobe of the mouse lung
- Heterogeneity of deposition patterns increases with increasing particle size
- Hot spots of deposition are mainly located in the apical region of the mouse lung

1
2
3
4
5
6
7
8
9

10 **Heterogeneity in lobar and near-acini deposition of inhaled aerosol in the mouse lung**
11

12
13

14 W. Gu and C. Darquenne*,
15

16
17
18
19
20
21
22

23 Department of Medicine, University of California, San Diego, USA
24

25
26
27
28
29
30

*Corresponding author: Chantal Darquenne, PhD

31
32
33
34
35
36
37
38

39 Department of Medicine
40

41
42
43
44
45
46
47
48
49
50
51
52
53
54
55
56
57
58
59
60
61
62
63
64
65

50 University of California, San Diego
51

52 9500 Gilman Drive, mail code 0623A
53

54 La Jolla, CA 92093-0623
55

56 USA
57

58 Email: cdarquenne@ucsd.edu
59

60
61
62
63
64
65

1
2
3
4
ABSTRACT
5
6

7 Laboratory animals are often used to derive health risk from environmental exposure or to assess
8 the therapeutic effect of a drug delivered by inhaled therapy. Knowledge of the in-situ distribution
9 of deposited particles on airway and alveolar surfaces is essential in any assessment of these effects.
10 A unique database including both high-resolution lung anatomy and deposition data in four strains
11 of laboratory mice have been recently made publicly available to the research community
12 (<https://doi.org/10.25820/9arg-9w56>). Using these data, we investigated the effect of particle size
13 on the distribution of deposited particles at the lobar and near-acini level. Analysis was performed
14 on a total of 33 mice where 3, 16 and 14 animals were exposed to 0.5 μ m, 1 μ m and 2 μ m particles,
15 respectively. Ratio of normalized deposition to normalized volume was calculated for each lobe
16 (DV_{lobe}). At the near-acini level, the skew and standard deviation of the frequency distribution of
17 particle deposition were calculated. Significant deviation above 1 was found for DV ratio in the
18 cranial lobe ($DV_{cranial}$). DV_{Middle} , DV_{Caudal} and $DV_{Accessory}$ were all significantly <1 and lower
19 than DV_{left} ($p<0.01$). At the near-acini level, skew and standard deviation were positively
20 correlated with particle size and the presence of hot spots (high deposition) were mainly found in
21 the apical region of the lung. These results highlight the uneven distribution of deposited particles
22 in the mouse lung. Thus, depending on the lung sample, individual analysis to determine overall
23 deposition may either underestimate or overestimate total lung burden, at least for micron-sized
24 particles.

25
26
27
28
29
30
31
32
33
34
35
36
37
38
39
40
41
42
43
44
45
46
47
48
49
50
51
52
53
54
55
56
Keywords: hot spots, spatial heterogeneity, particle deposition
57
58
59
60
61
62
63
64
65

1
2
3
4 **1. INTRODUCTION**
5
6
7
8
9
10
11
12
13
14
15
16
17
18
19
20
21
22
23
24
25
26
27
28
29
30

Exposure to airborne particulate matter (PM) plays an important role in initiating or aggravating respiratory and cardiovascular diseases. The understanding of the pathogenic effects resulting from such a PM exposure requires knowledge of the *in-situ* distribution of deposited pollutants on airway and alveolar surfaces. Such knowledge is also essential in any assessment of the therapeutic effect of a drug delivered by inhaled therapy. Animal models have long been used as surrogates to predict therapeutic effects in humans or to determine possible adverse health effects arising from chemical and/or particulate exposures. Mathematical models have often been used to complement experimental studies under different exposure conditions. In addition, modeling can also be used as a tool for interspecies dose extrapolation, an important element in preclinical and toxicological studies.

In recent years, sophisticated subject-specific computational models of aerosol transport and deposition in the lung have been developed for both humans (De Backer et al., 2008; Hofmann, 2011; Kuprat et al., 2020; Ma & Lutchen, 2009; Vinchurkar et al., 2012) and research animals (Asgharian et al., 2016; Kabilan et al., 2016). These models lack subject-specific experimental validation and have been mainly validated with averaged *in vivo* deposition data from the literature. As considerable inter-subject variability exists both in airway geometry and in deposition data, there is a need for detailed subject-specific datasets of lung anatomy and site-specific deposition information. Beichel et al. recently provided such data for the mouse lung in a publicly accessible repository, the lapdMouse archive (Beichel, Glenny, Bauer, Krueger, & Lamm, 2019). This archive provides high-resolution lung models of 34 mice combined with experimental data of local particle deposition and breathing parameters measured during aerosol exposure. These data may

not only be used to develop more accurate models of particle deposition in the mouse lung but can also be analyzed to better understand the interplay between lung anatomy and regional aerosol deposition among animals. The mouse is one of the most commonly used animal models in toxicological and preclinical studies. It is thus important to understand heterogeneities in deposition patterns not only within a single mouse lung but also across different strains. This is the focus of this study. In particular, we investigated the effect of particle size on the lobar distribution of aerosol deposition and also on deposition patterns at the near-acini level.

2. METHODS

2.1. Study data

The data used in this study were obtained from the Lung anatomy + particle deposition mouse (lapdMouse) archive that has been described in detail elsewhere (Bauer, Krueger, Lamm, Glenny, & Beichel, 2020). Briefly, this unique database includes high-resolution anatomical data of the lungs of 34 mice that are linked to three-dimensional (3D) particle deposition maps. Mice of both sexes and of four different strains (B6C3F1, BALB/C, C57BL/6 and CD-1) were exposed to fluorescent aerosol particles with diameters of 0.5, 1.0 or 2.0 μm while free breathing in nose-only exposure chambers (Table 1). Following exposure, the lungs of these mice were imaged in a serial block-face imaging cryomicrotome at various wavelengths to isolate deposited particles and lung structure. The images were then processed to identify the 3D airway geometry and location of deposited particles. The airways from the trachea to the terminal bronchi were identified, labeled and represented as a mesh. These data were compiled by Beichel et al. (Beichel et al., 2019) in the lapdMouse archive that can be accessed at <https://doi.org/10.25820/9arg-9w56>.

1
2
3
4
5 **Table 1.** Summary of samples from the lapdMouse archive
6

Particle Size	Strain and Sex								Total	
	B6C3F1		BALB/c		CD-1		C57BL/6			
	M	F	M	F	M	F	M	F		
0.5 µm	-	-	1	2	-	-	-	-	3	
1 µm	2	2	2	2	2	2	2	2	16	
2 µm	2	2	2	2	1	2	2	2	15	

24 M: male, F: female.
25
26
27
28

29 *2.2. Data analysis*
30

31 *2.2.1. Lobar deposition.*
32

33 In order to compare aerosol particle deposition densities across lobes, lobar volume (V_{lobe}) was
34 normalized by total lung volume (V_{total}) and lobar particle deposition (D_{lobe}) by total particle
35 deposition in the lung (D_{total}). The volume-normalized deposition fraction in each lobe (DV_{lobe})
36 was then calculated as the ratio between normalized lobar particle deposition and normalized lobar
37 volume, i.e.
38

39
40
41
42
43
44

$$DV_{lobe} = \frac{\frac{D_{lobe}}{D_{total}}}{\frac{V_{lobe}}{V_{total}}} \quad (1)$$

45
46
47
48
49
50
51 For each mouse sample, DV ratios were calculated for each lung lobe: left lobe, right cranial lobe,
52
53 right accessory lobe, right middle lobe and right caudal lobe and denoted as DV_{left} , $DV_{cranial}$,
54
55 $DV_{accessory}$, DV_{middle} and DV_{caudal} .
56
57
58
59
60
61
62
63
64
65

1
2
3
4 Since DV_{lobe} is the ratio of normalized particle deposition over normalized lobar volume, it is a
5 good indicator of lobar particle deposition density. If the number of deposited particles is
6 proportional to the lobar volume, DV_{lobe} ratio is one. If the density of deposited particles in a lobe
7 is higher than the averaged whole-lung deposition density, then DV_{lobe} is greater than one.
8
9 Inversely, if aerosol particles are sparsely deposited in a lobe, then DV_{lobe} is less than one.
10
11
12
13
14

15
16
17
18
19
20 *2.2.2. Near-acini deposition.*

21 Bauer et al. (Bauer et al., 2020) partitioned the lung of each mouse into near-acini structures of ~ 3
22 mm³ resulting in ~ 350 compartments/lung. For each mouse, we ranked these compartments based
23 on the density of deposited particles. Deposition densities (expressed in arbitrary units) ranged
24 from 0 to 4.75, with 99.8% of the compartment having a deposition density ≤ 4 . A forty-bin
25 frequency distribution of near-acini particle deposition was then constructed. Any compartment
26 with a deposition greater than four was considered an outlier and grouped together at the tail end
27 of the distribution. The standard deviation (SD) and third moment about the mean (skew, Sk) of
28 the distributions were then calculated:
29
30
31
32
33
34
35
36
37
38
39
40

41
42
43
44
$$SD = \frac{\sum_{i=1}^n (x_i - \bar{X})^2}{n} \quad (2)$$

45
46
47
48
49

50
$$Sk = \frac{\sum_{i=1}^n (x_i - \bar{X})^3}{n} \quad (3)$$

51
52
53
54
55
56
57
58

59 where n is the total number of near-acini compartments and \bar{X} is the average near-acini single-
60 compartment particle deposition.
61
62
63
64
65

The apex-to-base distribution of near-acini deposition was also calculated. For this analysis, each near-acini compartment location was identified by the distance of its centroid to a reference plane that intersects with the carina and is perpendicular to the bisector line between the main bronchi. Data were then plotted as a function of distance to the reference plane. Near-acini compartments with mean deposition equal to or higher than $Z_{0.01}$ standard deviations above the median were defined as hotspots and their spatial location was recorded.

2.3. Statistical Analysis.

DV_{lobe} ratios were grouped by particle size and strain. For each group, multiple two-tail T tests were performed to determine if DV_{lobe} ratios were significantly different from one. Paired five-way ANOVA tests were run to compare the differences of DV_{lobe} ratios across lobes. Unpaired ANOVA tests were run to compare if DV_{lobe} ratios were distinctive in different mouse samples with different strain, sex and particle size. DV_{lobe} ratios were also regressed on particle size. Tests with P values smaller than 0.05 were reported as significant.

The third moment and standard deviation of distributions of near-acini deposition were regressed on particle size. Unpaired T and ANOVA tests were performed to determine if distribution statistics were different across strains and sex. Tests with P values smaller than 0.05 were reported as significant.

1
2
3
4 **3. RESULTS AND DISCUSSION**
5
6
7
8
9
10
11
12
13

All datasets available in the lapdMouse archive were used in this study except for one (mouse m25, 2 μm aerosol) that was labeled as being of poor quality (quality C). Thus, analysis from 33 datasets are presented here.

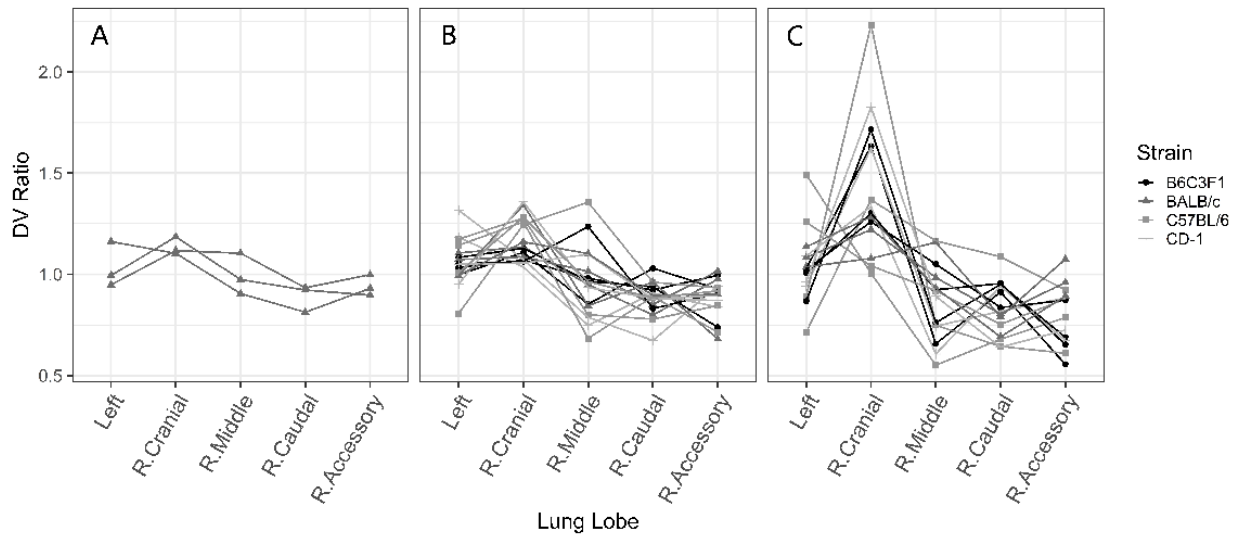
14
15
16
17
18 *3.1 Lobar deposition*
19
20

21 There was no significant effect of sex or strain on DV_{lobe} so data were group based on particle size.
22
23 DV_{lobe} ratios averaged over all mice exposed to a given particle size (mean \pm SD) are listed in
24 Table 2 and individual DV ratios are shown in Figure 1 where different strains are identified by
25 different symbols. There were variations in DV ratios among lobes and these variations increased
26 with increasing particle size. For mice exposed to 2 μm particles, significant deviation from 1 was
27 found for DV ratio in the cranial lobe ($DV_{Cranial}$), where deposition was relatively greater than
28 lobar volume ($P < 0.001$) while DV_{Middle} , DV_{Caudal} and $DV_{Accessory}$ were all significantly smaller
29 than one ($p = 0.020$, $p < 0.001$ and $p < 0.001$, respectively). Similar trends were found for animals
30 exposed to 1 μm particles, however significance was not reached for DV_{middle} . For animals
31 exposed to 0.5 μm particles, the only DV ratio that was significantly different than one was
32 $DV_{cranial}$ (>1 , $p = 0.033$). Finally, irrespective of particle size, DV_{left} showed no difference from
33 one, indicating that particle deposition in the left lobe is proportional to the lobar volume.
34
35
36
37
38
39
40
41
42
43
44
45
46
47
48
49
50
51
52
53
54
55
56
57
58
59
60
61
62
63
64
65

1
2
3
4 **Table 2.** Averaged *DV* ratio in the lung lobes for each particle size
5
6

Particle		size	N	DV ratio				
				Left	R. Cranial	R. Middle	R. Caudal	R. Accessory
0.5 μm	3	0.5 μm	3	1.04 \pm 0.11	1.14 \pm 0.04*	0.99 \pm 0.10	0.89 \pm 0.07	0.94 \pm 0.05
1 μm	16	1 μm	16	1.06 \pm 0.11	1.17 \pm 0.11*	0.96 \pm 0.18	0.88 \pm 0.08*	0.88 \pm 0.10*
2 μm	15	2 μm	15	1.04 \pm 0.18	1.42 \pm 0.34*	0.86 \pm 0.19*	0.82 \pm 0.13*	0.80 \pm 0.15*

N: number of samples; R.: Right; *: significantly different from 1 ($P<0.05$)



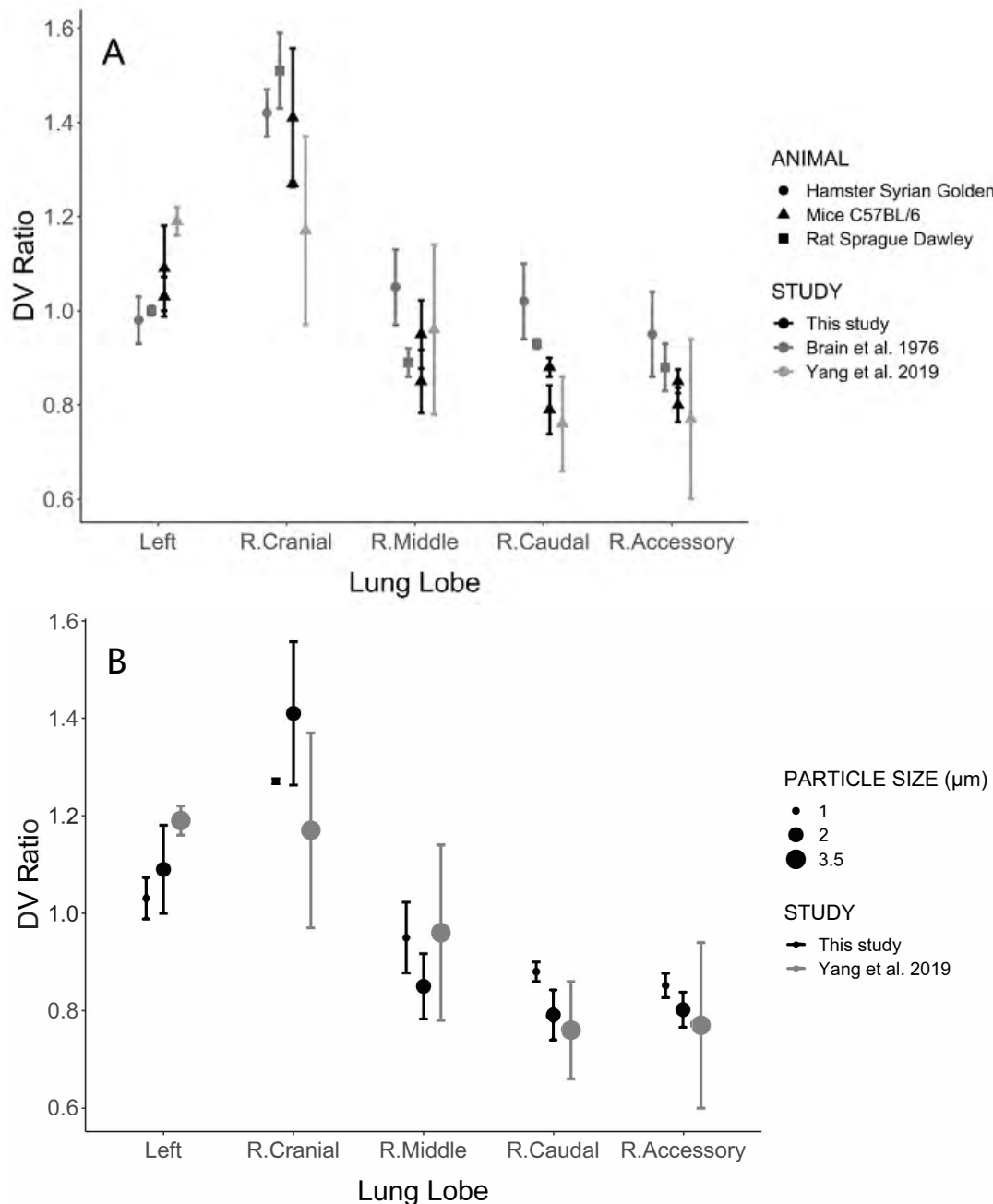
51 **Figure 1.** Individual *DV* ratio for each lobe of the mouse lung. A: 0.5 μm (N=3).
52
53 B: 1 μm (N=16). C: 2 μm (N=14). R.: right.
54
55
56
57
58
59
60
61
62
63
64
65

1
2
3
4 Data showed in Figure 1 and Table 2 compare well with previous studies in rodents. Brain and
5 colleagues (Brain, Knudson, Sorokin, & Davis, 1976) delivered aerosol (MMAD=1.6 μm) to both
6 Syrian golden hamsters and Sprague Dawley rats in animal exposure chambers and determined the
7 distribution of deposited particles through the evenness index (EI) defined as the ratio between
8 normalized lobar deposition and normalized lobe weight (Figure 2A). In both species, the EI was
9 larger than one in the cranial lobe (EI = 1.42 in hamsters and EI = 1.51 in rats) while EI in the left
10 lobe was close to one (EI = 0.98 in hamsters and EI=1 in rats). In rats, they also observed an EI <
11 1 in the right middle, right accessory and right caudal lobes. Morgan et al. (Morgan et al., 1983)
12 exposed SAS/4 mice to $^{239}\text{PuO}_2$ particles with a median aerodynamic diameter of 0.8, 1.5 and 2.2
13 μm . They observed EI larger than 1 in the cranial lobe and EI < 1 in the caudal and accessory lobe,
14 with deviations from one increasing with increasing particle sizes, in agreement with data from
15 this study (Table 2). Finally, in a more recent study, Yang and colleagues (Yang et al., 2019)
16 delivered a liquid aerosol with a volume median diameter of 3.5 μm by mechanical ventilation to
17 C57J/6 mice. Even though the particle size was larger than those used in this study, the *DV* ratio
18 in each lobe show similar behavior as those observed in the C57J/6 mice included in this study
19 (Figure 2B).

20
21
22
23
24
25
26
27
28
29
30
31
32
33
34
35
36
37
38
39
40
41
42
43
44
45
46

47 The distribution of deposited particles in the lung is closely linked to the distribution of inhaled air
48 among the different regions of the lungs (Bennett et al., 2002; Moller, Meyer, Scheuch, Kreyling,
49 & Bennett, 2009). In humans (Milic-Emili, Henderson, Dolovich, Trop, & Kaneko, 1966) and
50 large animals such as horses (Amis, Pascoe, & Hornof, 1984), the dependent lung region gets
51 proportionally a larger fraction of a tidal breath than the nondependent lung regions. In contrast,
52 in small animals such as the rat, the non-dependent lung region has been reported to be better
53
54
55
56
57
58
59
60
61
62
63
64
65

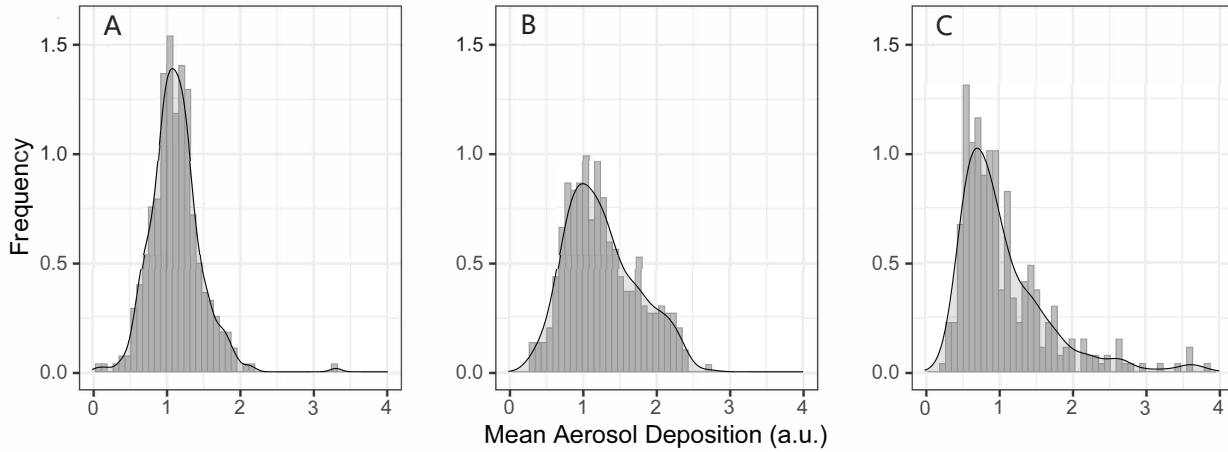
1
2
3
4 ventilated than the dependent lung region (Rooney, Friese, Fraser, Dunster, & Schibler, 2009).
5
6 This may explain the higher relative deposition in the non-dependent (cranial) than in the
7
8 dependent lobes of the right lung (accessory and caudal) of rodents.
9



57 **Figure 2.** DV ratio in each lobe of the lung. A: comparison with previous studies in
58 rodents (Hamster, mice and rats). B: effect of particle (mice only). R.: right.
59
60
61
62
63
64
65

1
2
3
4 3.1 Near-acini deposition:

5
6
7 The shape of the distribution of near-acini deposition was also affected by particle size. Mice
8 exposed to small aerosol particles ($0.5 \mu\text{m}$) tended to have a narrow, i.e. homogeneous, distribution
9 (Figure 3A). On the contrary, for mice exposed to larger aerosol particles (1 and 2 μm), the
10 distribution of near-acini deposition tended to be wider, indicating an increase in heterogeneity of
11 near-acini deposition with increasing particle size (Figures 3B and C).



37 **Figure 3.** Histograms of near-acini deposition in BALB/c mice. A: $0.5 \mu\text{m}$. B: 1
38 μm . C: $2 \mu\text{m}$.

41
42
43
44 The distributions of near-acini deposition were characterized by their standard deviation (SD) and
45 skew (Sk). Individual data for all 33 mice samples are plotted in Figure 4 against particle size.
46
47 Median, quartiles (box) and 95% intervals (vertical line) are also displayed in the figures. Both
48
49 standard deviation and skew significantly increased with increasing particle size. The rather small
50
51 standard deviation of near-acini deposition for $0.5 \mu\text{m}$ particles indicates a homogeneous
52
53 deposition throughout the lung for these small particles. These results also suggest that the
54
55
56
57
58
59
60
61
62
63
64

homogenous deposition observed at the lobar level still occur at the near-acini level for this small particle size.

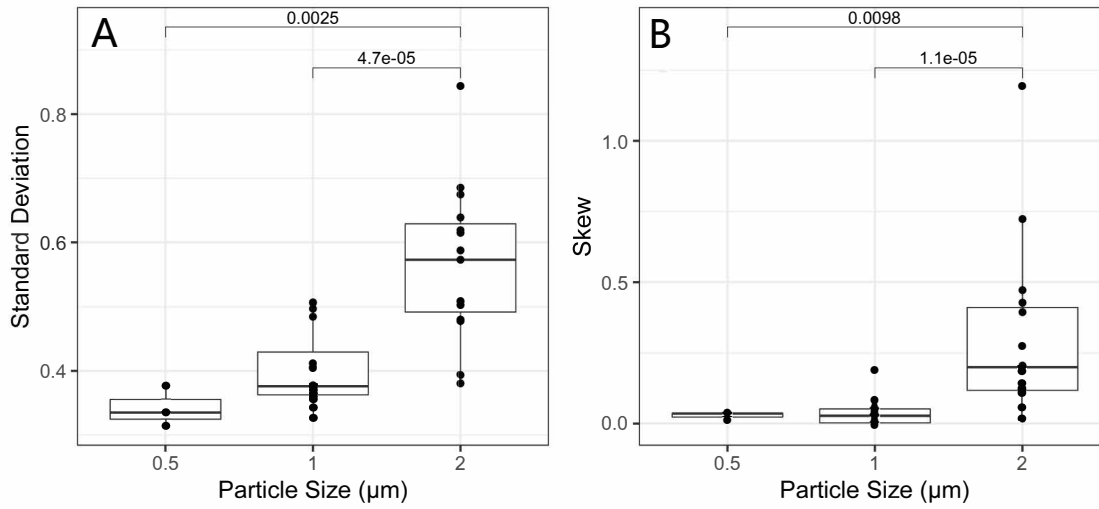


Figure 4. Parameters characterizing the near-acini deposition. Individual data are shown (closed symbols) along with the median and quartiles (box) and 95% confidence interval (vertical line). Significant p values are also shown. A: Standard deviation. B: Skew.

For all mice and particle size, skew was positive, i.e. the distribution was right-skewed. It has been previously shown that skew is a measure of hot spots of deposited particles. The larger the skew is, the more “hot spots” there are, i.e. the more there are near-acini units with higher particle deposition (hot spots) than expected from a normal distribution (Darquenne et al., 2013). Previous studies in humans showed that skew was inversely correlated with alveolar deposition (Garrard, Gerrity, Schreiner, & Yeates, 1981), implying that high values of skew are indicative of hot spots of deposited particles occurring predominantly in the bronchial airways. To our knowledge, there

1
2
3
4 are no reports of skew of deposition distribution in rodents. Figures 5A-C display the location of
5 the top 1% of near-acini deposition relative to the airway tree structure for mice exposed to 0.5, 1
6 and 2 μm particles, respectively. Interestingly, the hot spots, while located relatively centrally,
7 were only present in the apical region of the lungs, i.e. in the right cranial lobe and in the upper
8 portion of the left lobe. There was also a significant effect of height on near-acini deposition with
9 deposition being on average higher near the apex of the lung than towards the base of the lung (Fig.
10 5D-F). The slopes of the regression lines were all significant ($p<0.001$) and increased with
11 increasing particle size. Data shown in Figure 5 are from the same BALB/c mice as those used in
12 Figure 3 but similar distributions of near-acini deposition were found in all of the 33 samples but
13 one.
14
15
16
17
18
19
20
21
22
23
24
25
26
27
28
29
30

31 These observations may explain the higher deposition measured in the right cranial lobe (Figure
32 1). As discussed above, the non-dependent region of the rodent lung is better ventilated than the
33 dependent region. Because there is no major difference in the diameter of the airway of a given
34 generation between lobes (data not shown), higher ventilation in the apical region of the lung
35 results in higher velocities in the airways from the apical region than in similar airways located at
36 the base of the lung. These high velocities increase the probability of a particle depositing by
37 inertial impaction at airway bifurcation and thus increase the potential for the generation of hot
38 spots. Indeed, of the three main mechanisms of aerosol deposition in the lung (inertial impaction,
39 gravitational sedimentation and Brownian diffusion), inertial impaction is the only velocity-
40 dependent mechanism (Darquenne, 2012).
41
42
43
44
45
46
47
48
49
50
51
52
53
54
55
56
57
58
59
60
61
62
63
64
65

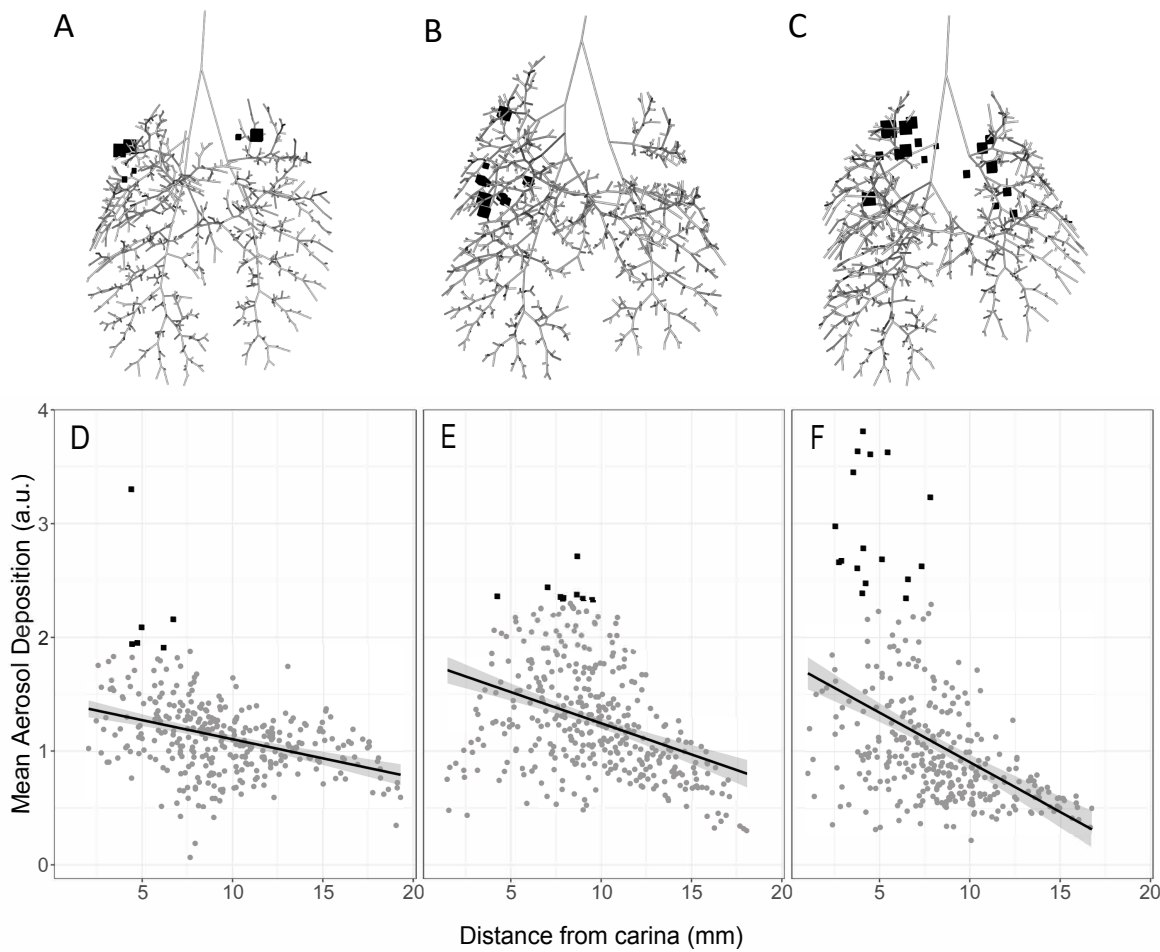


Figure 5. Spatial location of the top 1% near-acini deposition (hot spots) and apex-to-base distribution of near-acini deposition in the same BALB/c mice as in Figure 3. Hot spots were mainly located toward the apex of the lung (identified by black squares in all panels). A, D: 0.5 μm . B, E: 1 μm . C, F: 2 μm . See text for details.

4. SUMMARY

Analysis was performed on the newly available lapdMouse archive to determine the heterogeneity of aerosol deposition at the lobar and near-acini scale in the mouse lung. The distribution of deposited particles among lobes was uneven with deposition in the cranial lobe being relatively

1
2
3
4 greater than lobar volume and deposition in the middle, caudal and accessory lobes being relatively
5 lower than their volume. There was also a particle size effect on lobar deposition unevenness that
6 increased with increasing particle size (0.5 – 2 μm). At the near-acini level, larger particle size was
7 associated with a less uniform spatial distribution of particle deposition and a higher likeness of
8 formation of hot spots mainly in the apical region of the lung.
9
10
11
12
13
14

15 16 17 18 **ACKNOWLEDGEMENTS** 19 20

21 The study was funded by the National Institutes of Health (U01ES028669 from the NIEHS).
22
23
24
25
26

27 28 **DECLARATION OF INTERESTS** 29 30

31 The authors declare that they have no known competing financial interests or personal
32 relationships that could have appeared to influence the work reported in this paper.
33
34
35
36
37
38
39
40
41
42
43
44
45
46
47
48
49
50
51
52
53
54
55
56
57
58
59
60
61
62
63
64
65

1
2
3
4 **REFERENCES**
5
6
7
8
9
10
11
12
13
14
15
16
17
18
19
20
21
22
23
24
25
26
27
28
29
30
31
32
33
34
35
36
37
38
39
40
41
42
43
44
45
46
47
48
49
50
51
52
53
54
55
56
57
58
59
60
61
62
63
64
65

- Amis, T. C., Pascoe, J. R., & Hornof, W. (1984). Topographic distribution of pulmonary ventilation and perfusion in the horse. *Am J Vet Res*, 45, 1597-1601.
- Asgharian, B., Miller, F. J., Price, O., Schroeter, J. D., Einstein, D. R., Corley, R. A., & Bentley, T. (2016). Modeling particle deposition in the pig respiratory tract. *Journal of Aerosol Science*, 99, 107-124.
- Bauer, C., Krueger, M. A., Lamm, W. J., Glenny, R. W., & Beichel, R. R. (2020). lapdMouse: associating lung anatomy with local particle deposition in mice. *Journal of Applied Physiology*, 128, 309-323.
- Beichel, R. R., Glenny, R. W., Bauer, C., Krueger, M. A., & Lamm, W. J. (2019). Lung anatomy + particle deposition (lapd) mouse archive. University of Iowa.
- Bennett, W. D., Brown, J. S., Zeman, K. L., Hu, S. C., Scheuch, G., & Sommerer, K. (2002). Targeting delivery of aerosols to different lung regions. *J Aerosol Med*, 15, 179-188.
- Brain, J. D., Knudson, D. E., Sorokin, S. P., & Davis, M. A. (1976). Pulmonary distribution of particles given by intratracheal instillation or by aerosol inhalation. *Environmental Research*, 11, 13-33.
- Darquenne, C. (2012). Aerosol deposition in health and disease. *J Aerosol Med Pulm Drug Deliv*, 25, 140-147. doi: DOI: 10.1089/jamp.2011.0916
- Darquenne, C., Zeman, K. L., Sa, R. C., Cooper, T. K., Fine, J. M., Bennett, W. D., & Prisk, G. K. (2013). Removal of sedimentation decreases relative deposition of coarse particles in

1
2
3
4 the lung periphery. *Journal of Applied Physiology*, 115, 546-555. doi:
5
6 doi:10.1152/japplphysiol.01520.2012
7
8
9

10 De Backer, J. W., Vos, W. G., Gorle, C. D., GermonprC, P., Partoens, B., Wuyts, F. L., . . . De
11
12 Backer, W. (2008). Flow analyses in the lower airways: Patient-specific model and
13
14 boundary conditions. *Med. Eng. Phys.*, 30, 872-879.
15
16
17
18

19 Garrard, C. S., Gerrity, T. R., Schreiner, J. F., & Yeates, D. B. (1981). The characterization of
20
21 radioaerosol deposition in the healthy lung by histogram distribution analysis. *Chest*,
22
23 80(suppl), 840-842.
24
25
26

27 Hofmann, W. (2011). Modeling inhaled particle deposition in the human lung: A review. *Journal*
28
29 of *Aerosol Science*, 42, 693-724.
30
31
32

33 Kabilan, S., Suffield, S. R., Recknagle, K. P., Jacob, R. E., Einstein, D. R., Kuprat, A. P., . . .
34
35 Corley, R. A. (2016). Computational fluid dynamics modeling of Bacillus anthracis spore
36
37 deposition in rabbit and human respiratory airways. *Journal of Aerosol Science*, 99, 64-
38
39 77.
40
41
42

43 Kuprat, A. P., Jalali, M., Jan, T., Corley, R. A., Asgharian, B., Price, O., . . . Darquenne, C.
44
45 (2020). Efficient bi-directional coupling of 3D Computational Fluid-Particle Dynamics
46
47 and 1D Multiple Path Particle Dosimetry lung models for multiscale modeling of aerosol
48
49 dosimetry. *J Aerosol Sci, submitted to special issue*.
50
51
52

53 Ma, B., & Lutchen, K. R. (2009). CFD simulation of aerosol deposition in an anatomically based
54
55 human large-medium airway model. *Annals of Biomedical Engineering*, 37, 271-285.
56
57
58
59
60
61
62
63
64
65

1
2
3
4 Milic-Emili, J., Henderson, J. A. M., Dolovich, M. B., Trop, D., & Kaneko, K. (1966). Regional
5
6 distribution of inspired gas in the lung. *Journal of Applied Physiology*, 21, 749-759.
7
8
9

10 Moller, W., Meyer, G., Scheuch, G., Kreyling, W. G., & Bennett, W. D. (2009). Left-to-right
11
12 asymmetry of aerosol deposition after shallow bolus inhalation depends on lung
13
14 ventilation. *J Aerosol Med Pulm Drug Deliv*, 22, 333-339.
15
16
17

18 Morgan, A., Black, A., Moores, S. R., Pritchard, J. N., Walsh, M., & Lambert, B. E. (1983).
19
20 Alveolar Deposition of Sized Particles of $^{239}\text{PuO}_2$ in the Mouse. *Radiation Research*,
21
22 93, 85-92.
23
24
25

26 Rooney, D., Friese, M., Fraser, J. F., Dunster, K. R., & Schibler, A. (2009). Gravity-dependent
27
28 ventilation distribution in rats measured with electrical impedance tomography.
29
30
31 *Physiological Measurement*, 30, 1075-1085.
32
33
34

35 Vinchurkar, S., De Backer, L., Vos, W., Van Holsbeke, C., De Backer, J., & De Backer, W.
36
37 (2012). A case series on lung deposition analysis of inhaled medication using functional
38 imaging based computational fluid dynamics in asthmatic patients: Effect of upper
39
40 airway morphology and comparison with in-vivo data. *Inhalation Toxicology*, 24, 81-88.
41
42
43
44

45 Yang, L., Feuchtinger, A., Moller, W., DIng, Y., Kutschke, D., Moller, G., . . . Schmid, O.
46
47 (2019). Three-Dimensional Quantitative Co-Mapping of Pulmonary Morphology and
48 Nanoparticle Distribution with Cellular Resolution in Nondissected Murine Lungs. *ACS*
49
50 *Nano*, 13, 1029-1041.
51
52
53
54
55
56
57
58
59
60
61
62
63
64
65

1
2
3
4 **FIGURE LEGENDS**
5
6
7
8
9
10
11
12
13
14

Figure 1: Individual DV ratio for each lobe of the mouse lung. A: 0.5 μm (N=3). B: 1 μm (N=16). C: 2 μm (N=14). R.: right.

Figure 2: DV ratio in each lobe of the lung. A: comparison with previous studies in rodents (Hamster, mice and rats). B: effect of particle (mice only). R.: right.

Figure 3: Histograms of near-acini deposition in BALB/c mice. A: 0.5 μm . B: 1 μm . C: 2 μm .

Figure 4: Parameters characterizing the near-acini deposition. Individual data are shown (closed symbols) along with the median and quartiles (box) and 95% confidence interval (vertical line). Significant p values are also shown. A: Standard deviation. B: Skew.

Figure 5: Spatial location of the top 1% near-acini deposition (hot spots) and apex-to-base distribution of near-acini deposition in the same BALB/c mice as in Figure 3. Hot spots were mainly located toward the apex of the lung (identified by black squares in all panels). A, D: 0.5 μm . B, E: 1 μm . C, F: 2 μm . See text for details.

Figure 1

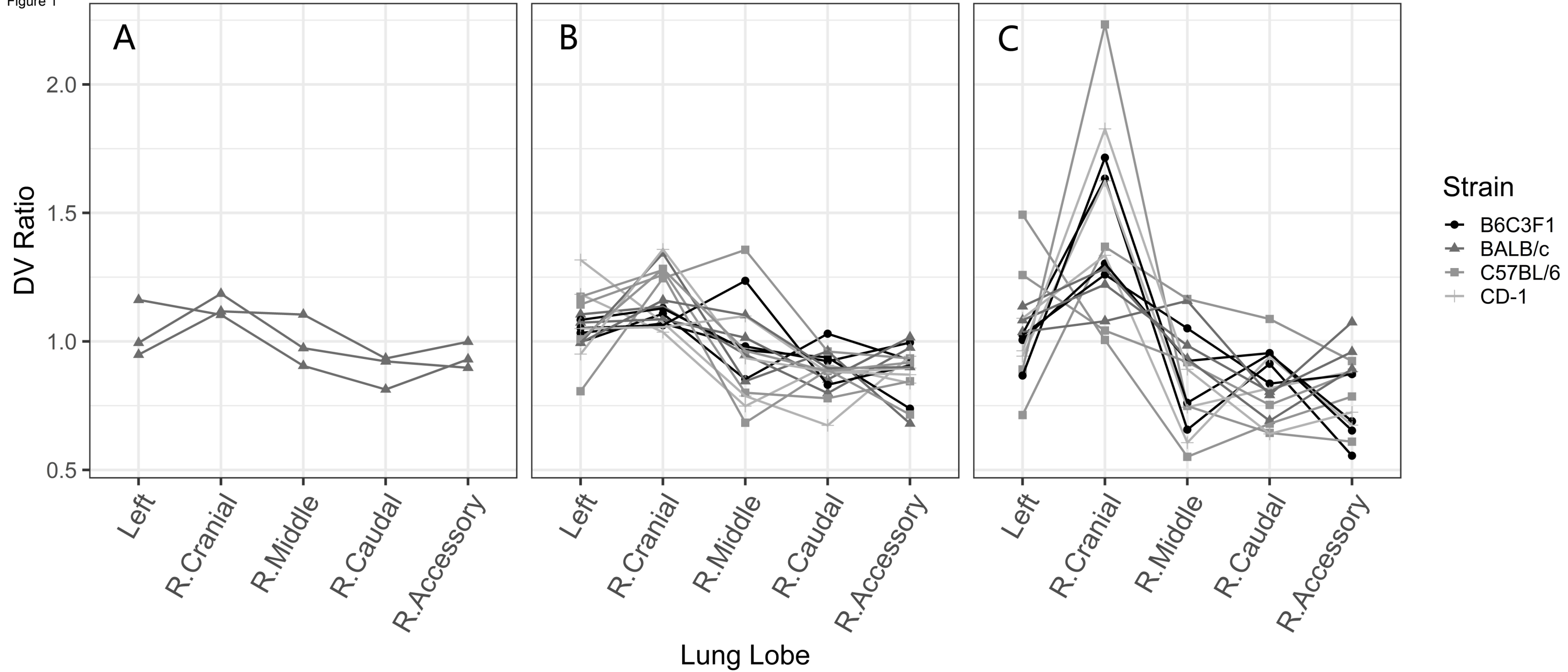


Figure 2A

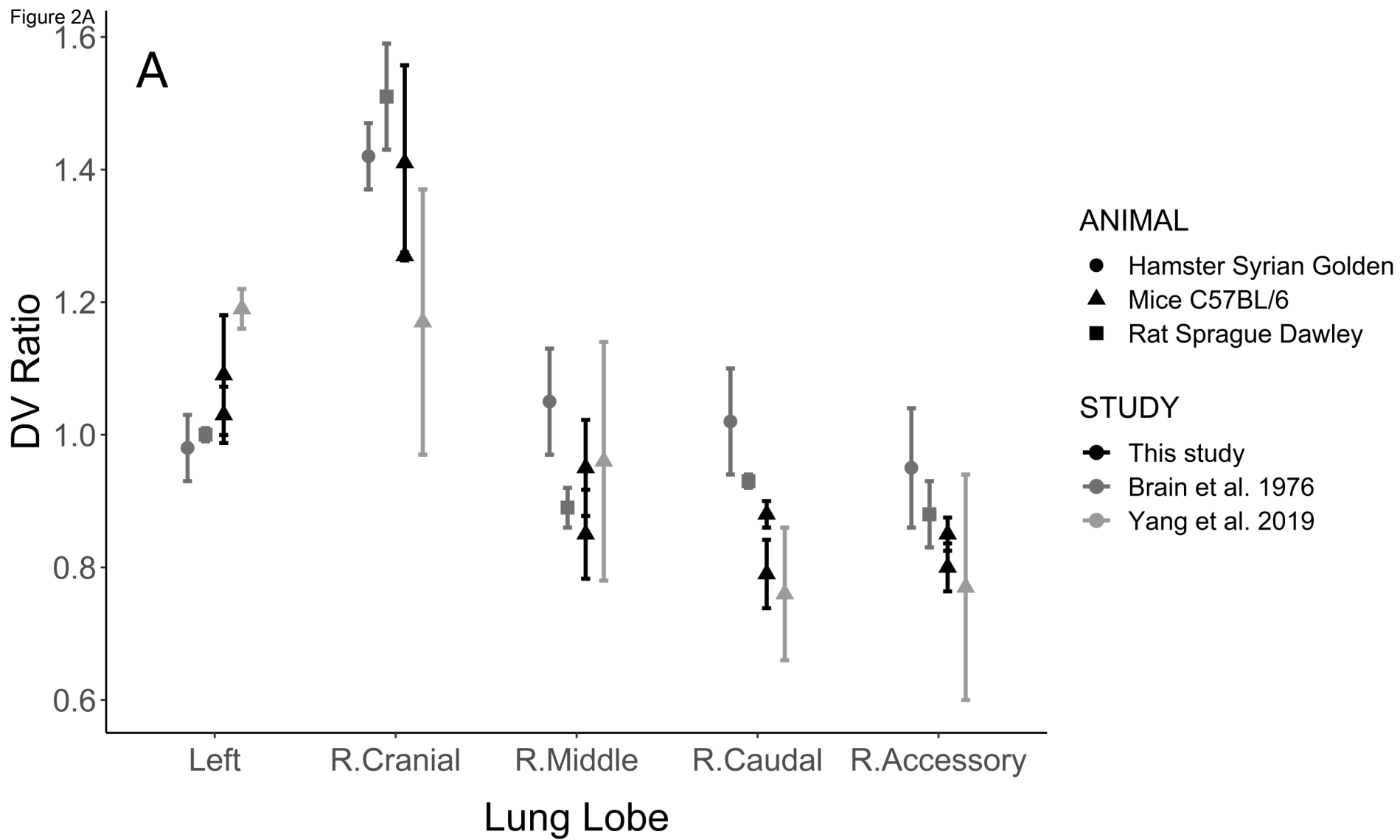


Figure 1B

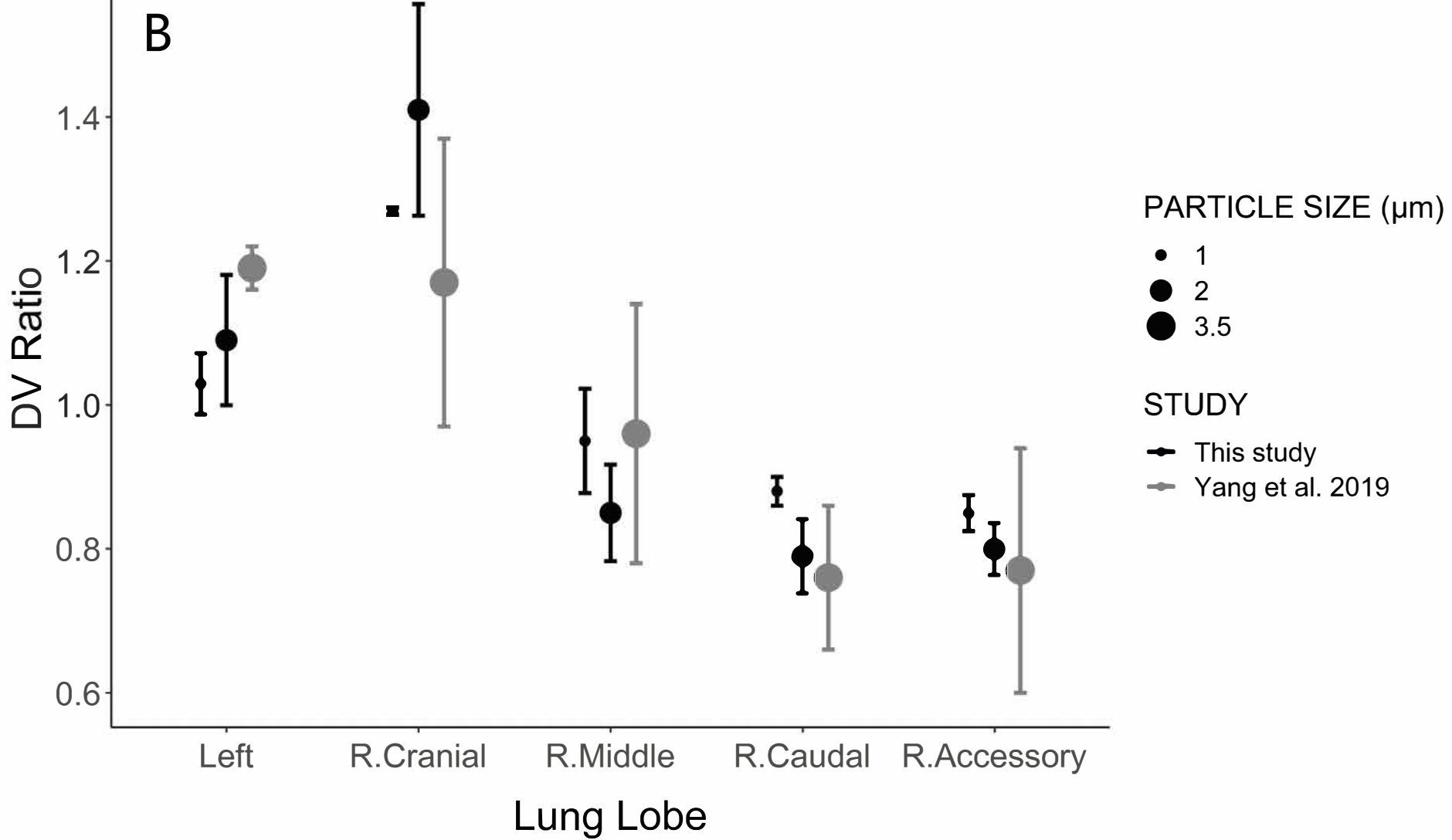


Figure 3

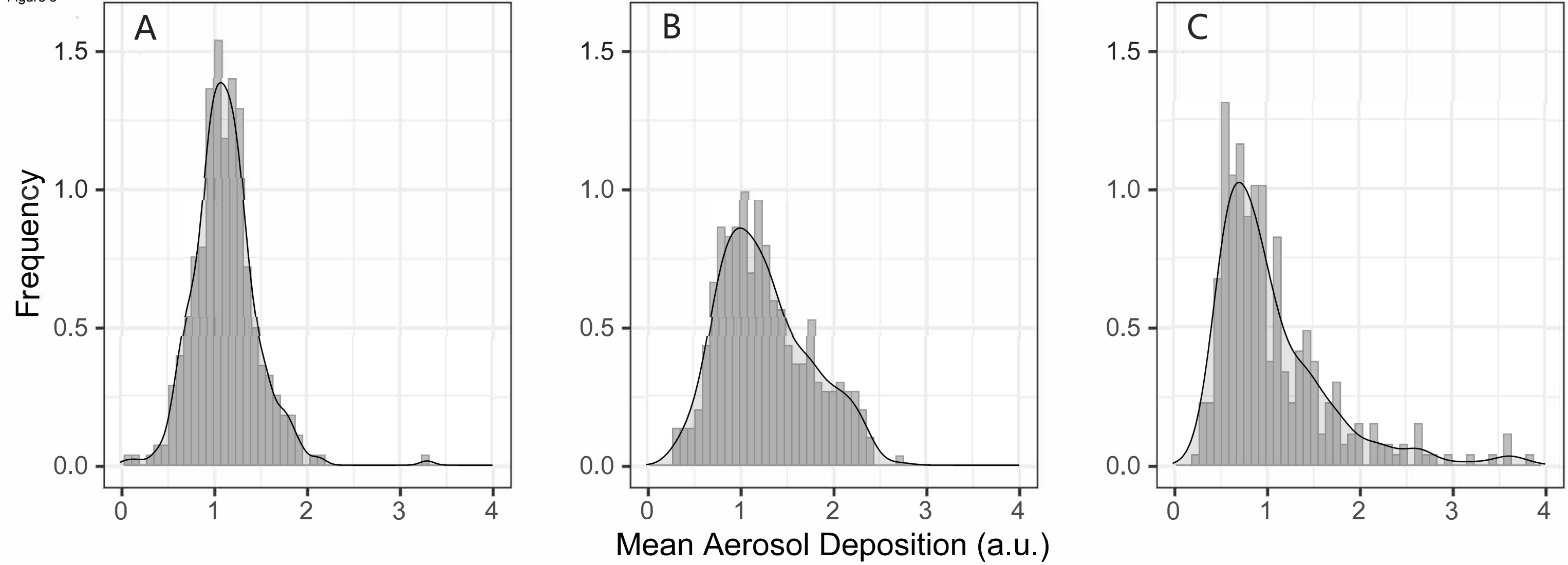


Figure 4

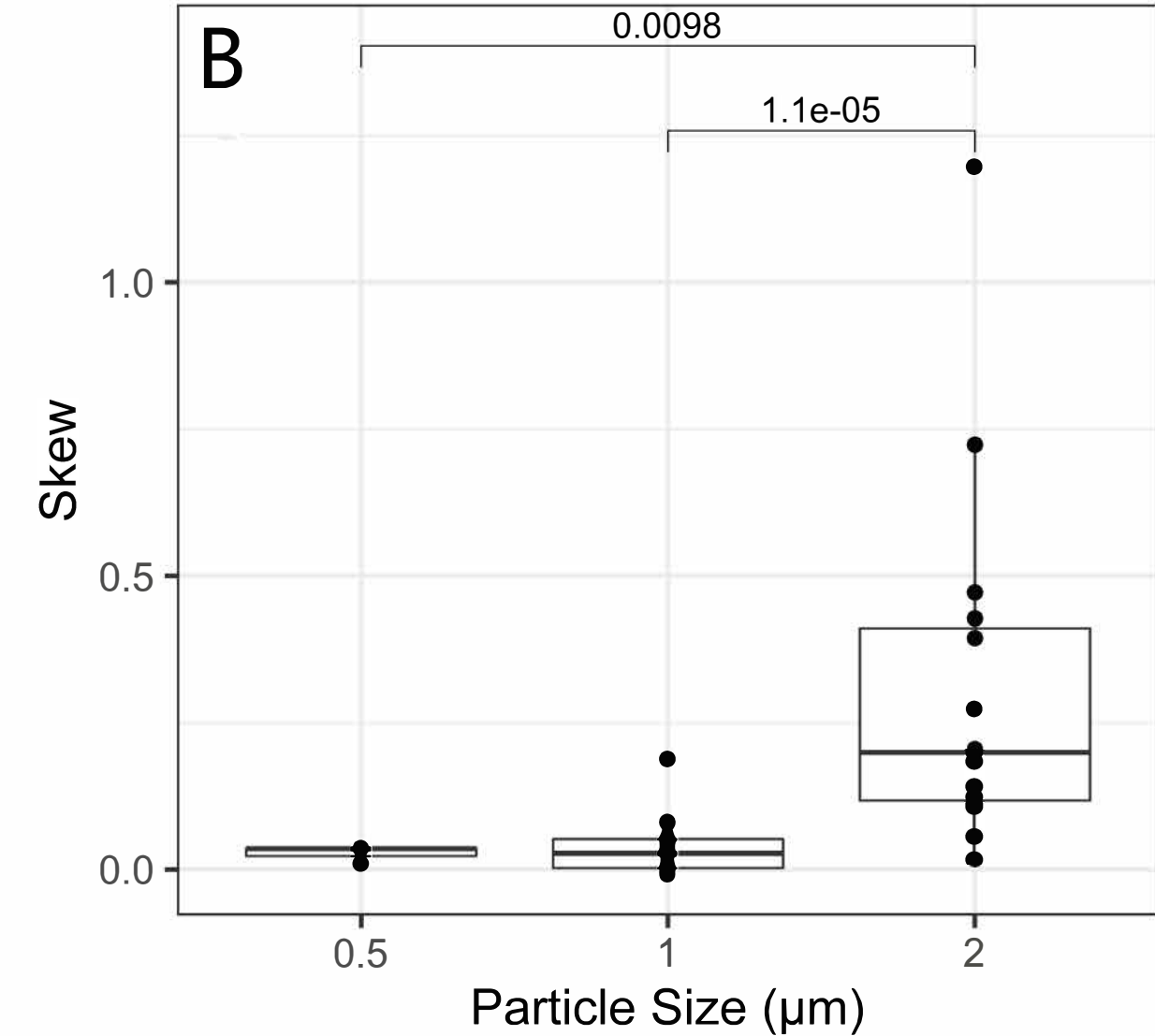
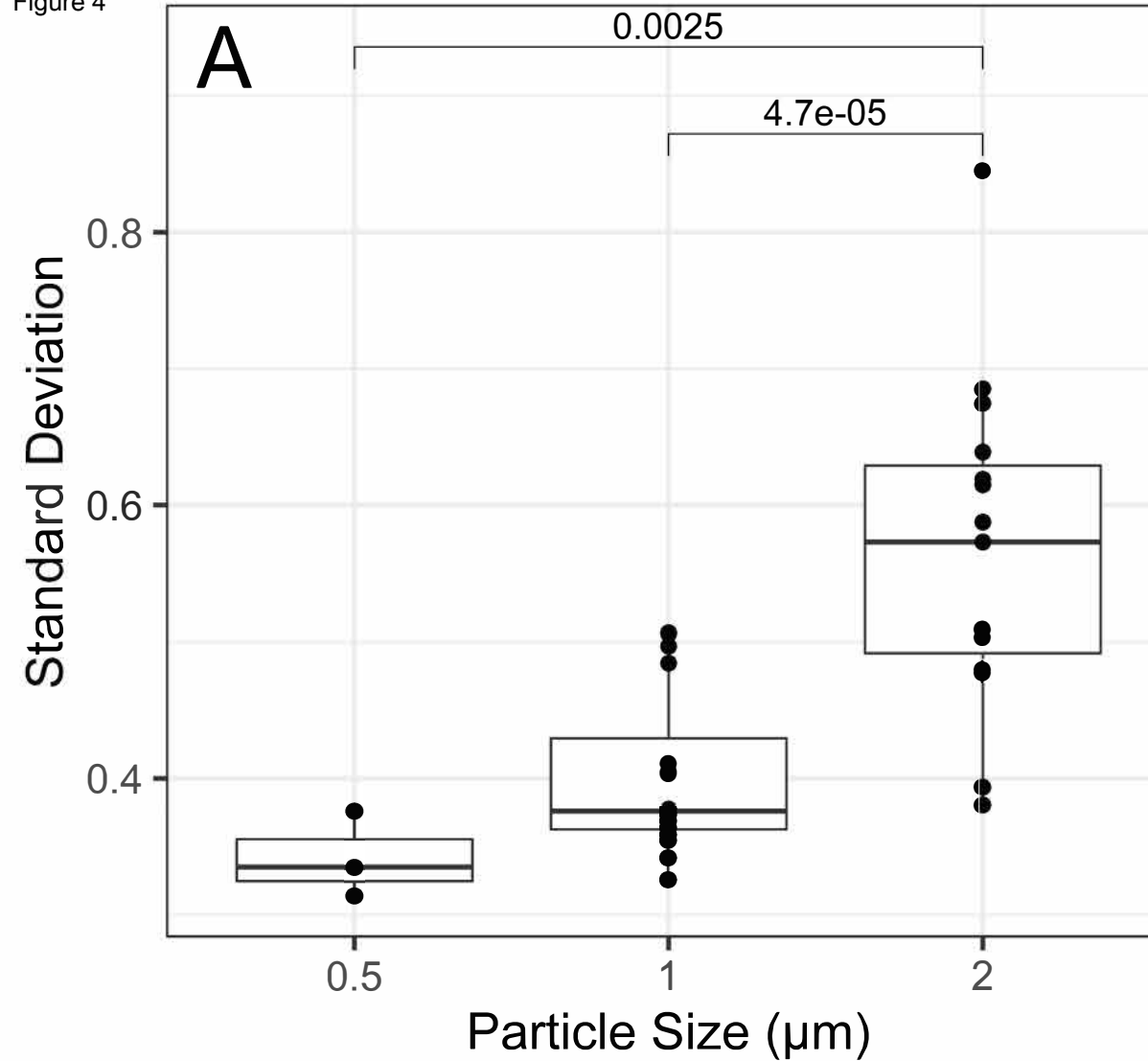


Figure 5

